

# Insights on structure and influence from the adjacency and Laplacian eigenspectra of intersecting ring networks

Agathe Bouis\*, Ruairidh A. Clark, Malcolm Macdonald

Applied Satellite Technology Laboratory, Department of Electronic and Electrical Engineering, University of Strathclyde, Glasgow, UK.

## ABSTRACT

Synchronisation is a pervasive phenomenon of emerging collective behaviour observed to develop spontaneously across both natural and engineered systems. The process and patterns of synchronisation are highly influenced by initial conditions and network topology. Synchronisation follows a network's hierarchical structure; developing first at a local level before conglomeration of local clusters typically drives synchronisation at a global scale. The structure and influence of both global and local features play a key role in node synchronisation. These differing insights are shown to be uncovered through eigenspectra analyses of ring networks. These network topologies exhibit complex patterns of stable and unstable synchronisation – despite apparently simple coupling schemes – as well as distinctive spectral fingerprints. Intersecting ring networks, with a common focal point, combine to produce hubs of high connectivity at the intersections whose network spectral analyses can denote the characteristics and distinctions of structure and influence. The adjacency eigenspectrum detects salient network structures, for example hubs of high connectivity, whilst the Laplacian spectrum identifies the relative influence of nodes due to their associated spanning trees within the network constituent structures.

**Key words:** Eigenspectrum analysis, Adjacency matrix, Laplacian matrix, Spectrum, Spectral clustering, Ring network, Circulant graph.

## I. INTRODUCTION

Structure and influence are herein defined as two complementary approaches to decomposing and understanding networks and their topologies. Structure considers the community clustering that emerges from variation in the relative density of connectivity between sets of nodes. Influence refers to a node's ability to affect the dynamical state of other nodes due to its position within the network's topology. The interplay of structure

and influence play a key role in a network's ability to achieve synchronisation of its nodes' state values, with the process being highly sensitive to both initial conditions and network topology [1].

Synchronisation is a phenomenon which occurs naturally across social, biological, and engineered networks [2], bringing together the fields of network science and chaos dynamics [3, 4]. Complex networks exhibit different patterns of synchronisation dependent on topology [1, 5].

---

\* Contact author: [agathe.bouis@strath.ac.uk](mailto:agathe.bouis@strath.ac.uk)

Three key patterns are distinguished [6]: global synchronisation, where all nodes follow the same state trajectory, partial synchronisation, where a limited number of nodes synchronise, and chimera states, where the networks evolves into dynamic patterns of coherence and incoherence [7, 8]. The impact of topology on synchronisation is exemplified by cluster synchronisation; where clusters, that is groups of nodes with a high connectivity density within the group and only sparse connections outwith [9, 10], see their nodes synchronise with nodes in their groups but not with other network nodes [11].

The influence of topology on synchronisation regimes can be investigated through eigenspectrum analyses [12]. This type of analysis is commonly used for community detection, that is, partitioning a network into community subgraphs which represent the functional entities acting on the network [12, 13]. Synchronisation follows these hierarchical scales, with synchronisation starting at a local level and building to the global [12]. Compared to the more commonly used statistical methods, such as, degree distribution, average degree, centrality, and modularity, eigenspectra analyses have proven to be a more effective at determining network dynamics and features [14, 15]. Graph characteristics, including their structural, connectivity, and clustering patterns are uncovered by assessing a graph's eigenspectrum [16]. This spectrum or arrangement of eigenvalues can be computed from a number of graph representation matrices, most commonly its adjacency or Laplacian matrix [17]. The choice of the representation matrix affects the detected spectrum, and the insights gained. However, to the best of the authors' knowledge, no clear insight has previously been established regarding which

matrix might provide the most relevant information.

Rings networks – also known as circulant graphs, star-polygon graphs, cyclic graphs, distributed loop networks, chordal rings, or multiple fixed step graphs – are of high interest to mathematics and engineering due to noteworthy synchronisation patterns, along with characteristic and distinct eigenspectra. Ring networks represent a special case of weak network coupling where each node is connected to its  $\delta$  nearest neighbours [18]. These topologies appear deceptively simple and yet, as they form closed loops of signal transmission with a signal being able to cycle across the network to come back to its node of origin, they have proven to be dynamically complex [19]. Ring networks can see the emergence of stable or unstable synchronisation, partial synchronisation, or even nonlinear chimera states due to their unique topology [20, 21]. It was found through the study of Kuramoto oscillators that there exists a coupling strength for which ring networks can be guaranteed to be globally synchronised, the state of interest for most engineered networks, below which the system's behaviour is expected to be incoherent [22, 23]. Circulant graphs' straightforward coupling scheme are also notable for their simplicity, expandability, and regularity [24]. These attributes have made them the subject of intense research in computer science, discrete mathematics, and engineering (see [18] and references therein), with key applications in the fields of computer networks and telecommunications. They have also found more recent applications in the space sector. Satellites equipped with Inter-Satellite Link (ISL) transmitters can communicate when in range of each other, enabling the creation of time-varying networks from the contacts between satellites.

Among the most common topologies of satellite networks are “string of pearls” [25], and Walker-delta constellations [26], both of which see ring networks as their underlying topographies. The former forms simple rings of interconnected satellites and the latter comprises intersecting rings [25].

Excluding their applications in satellite constellations, intersecting ring networks provide intuitive case studies to investigate the impact of network topology on synchronisation along with the topological features uncovered by spectral analysis. Intersecting ring networks combine the properties of rings, including their low connectivity and loops of signal transmission, with hubs of high connectivity at the rings’ intersections. This topology in turn brings together two complex chaotic phenomena: incoherent ring synchronisation with the networks’ arcs and cluster synchronisation at the rings’ intersections. Together this presents a unique challenge as real-life intersecting ring networks such as those of Walker-Delta satellite constellations typically require global synchronisation to secure their communications and navigation performance [27]. With current research focusing on the provision of distributed global time synchronisation in satellite networks [27, 28], understanding the topology, structure and influence, of intersecting ring networks is key to better understanding these networks’ processes and patterns of synchronisation. Herein, networks of intersecting rings such as those of Walker-Delta constellations are studied through their adjacency and Laplacian eigenspectra. The differing spectral insights obtained from the two representation matrices is compared. This comparison is facilitated by the rings having distinct and recognisable eigenspectra, making the comparison of

adjacency- and Laplacian-based analyses more intuitive.

## II. METHODOLOGY

The topology of an undirected, unweighted network,  $G = (E, \mathcal{E}, A)$ , can be described with a finite number of nodes (agents)  $E = \{1, 2, \dots, N\}$  and a set of directed edges  $\mathcal{E} \subseteq \mathcal{W} \times \mathcal{W}$ . Each directed edge  $(j, i) = (i, j) \in \mathcal{E}$  represents a link between the node pair  $(j, i)$ , such that communication between the nodes is enabled. The existence of edges is captured in the adjacency matrix  $A = [a_{ij}]_{N \times N}$ , where  $a_{ij} = 1$  denotes an edge. A node  $i$ ’s degree is indicated as  $\delta^i$ . Adapted from the adjacency matrix, the standard Laplacian matrix is defined as  $L = (D - A)$ , where  $D$  is a diagonal matrix whose diagonal elements  $D_{ii} = \delta^i$  are the degree of the node  $i$ .

### A. Community Detection

A network’s spectrum is herein defined as the sorted eigenvalues of the adjacency and Laplacian matrices, giving the adjacency spectrum and Laplacian spectrum, respectively. These eigenvalues are sorted in descending order, that is,  $\lambda_1^M \geq \lambda_2^M \geq \dots \geq \lambda_n^M$ . The eigenvalues’ associated eigenvectors are sorted in a similar fashion, resulting in an eigenvector matrix,  $\mathbb{V}^M$ , where  $M$  represents the matrix of choice, the adjacency,  $A$ , or the Laplacian,  $L$ . Note that for regular networks, meaning networks’ whose nodes have the same connectivity, the adjacency and Laplacian spectra are the same. Eigengaps are calculated for both the adjacency and Laplacian as the difference between adjacent eigenvalues,

$$\Delta\lambda_{12}^M = \lambda_1^M - \lambda_2^M. \quad (1)$$

The number of communities in which the network can most easily be partitioned into is

indicated by the index of the largest eigengap  $\text{idx}(\Delta\lambda_{\max}^M)$  [17], with most networks portioning in sets of interlocked, interacting, nested communities acting at different scales [29].

Further analysis of the network properties can be conducted by examining the Laplacian matrices' eigenvectors. The eigenvectors can be examined through heatmap plotting which highlight the influence of nodes, and through the plotting of the vector-wise norm of those same eigenvectors over the networks. The latter allows for truncated eigenvector matrices of interest to be explored. The influence of a range of eigenvectors are shown on the network plot, highlighting which nodes have the most effect on other nodes' dynamical state. The matrices analysed correspond to sections of the eigenvector heatmap of interest, for example, the eigenvectors of all nodes between rank  $i = 1$  and the rank of the most significant eigengap,  $\text{idx}(\Delta\lambda_{\max}^L)$ . The vector-wise norm of this submatrix ( $\mathbb{T}$ ) is

$$\mathbb{T} = \mathbb{V}_{n \times n} \rightarrow \mathbb{V}_{n \times (y-x)}, \quad (2)$$

$$\mathcal{U} = \left[ \sum_{k=x}^y |\mathbb{T}_k|^2 \right]^{\frac{1}{2}}, \quad (3)$$

where  $x$  and  $y$  are respectively the first and last indices of the eigenvector submatrix of interest, and  $\mathcal{U}$  is the vector-wise normalised value associated with the node, it has a size  $1 \times n$ , and takes on values between  $[0, 1]$ . The results of the vector wise normalisation are shown over the network plot; nodes with the most influence taking on values closer to 1 as they are influential across many of the eigenvector's columns. Nodes with the least influence take on values tending toward 0.

## B. Ring Eigenspectrum

It is important to understand the seemingly simple spectra of single ring networks before delving into the more complex networks motivating this research. Ring networks have simple coupling schemes and scalability, yet display chaotic synchronisation phenomena due to signal looping. Graph data can be analysed using common signal processing techniques: a graph signal is a vector of data, with each entry corresponding to a node data point. Graph frequencies are evaluated based on how node data change between nodes. The underlying network thus defines how the frequencies are calculated, with changes in topology impacting local variations [30]. In turn, these frequencies can be analysed using signal processing methods. Rings networks, with their circulant matrix where each row is a circular shift from the previous row [31], act as a circular convolution operator to any signal implemented upon them, with the eigenvectors of the network being, in fact, the columns of the Discrete Fourier Transform (DFT). Through this process, the signal, meaning the nodes' data, is effectively viewed as one period of length  $n$  (number of nodes) [30]. Much like the columns of the DFT matrix representing equal partitions of the unit circle [30], the eigenvectors of the network's Laplacian take on the values of the primitive root of unity [32],

$$\mathbb{V}^M = \exp\left(\frac{2\pi i}{n}\right). \quad (4)$$

As a result, for real-symmetric circulant matrices, eigenvalues come into pairs except for the first dominant eigenvalue, with the real and imaginary components of the primitive roots of unity splitting across two sets of eigenvectors. More practically speaking, this results in the network's eigenspectrum displaying stepped

behaviour as eigenvalues one and two, three and four, and so forth, are identical. As ring networks are regular networks, their adjacency and Laplacian spectrums are identical. The adjacency spectra and eigengap spectra of a 100-node ring's spectrum with different connectivity levels,  $\delta_R = \{2, 4, 6\}$  are shown in Fig. 1.

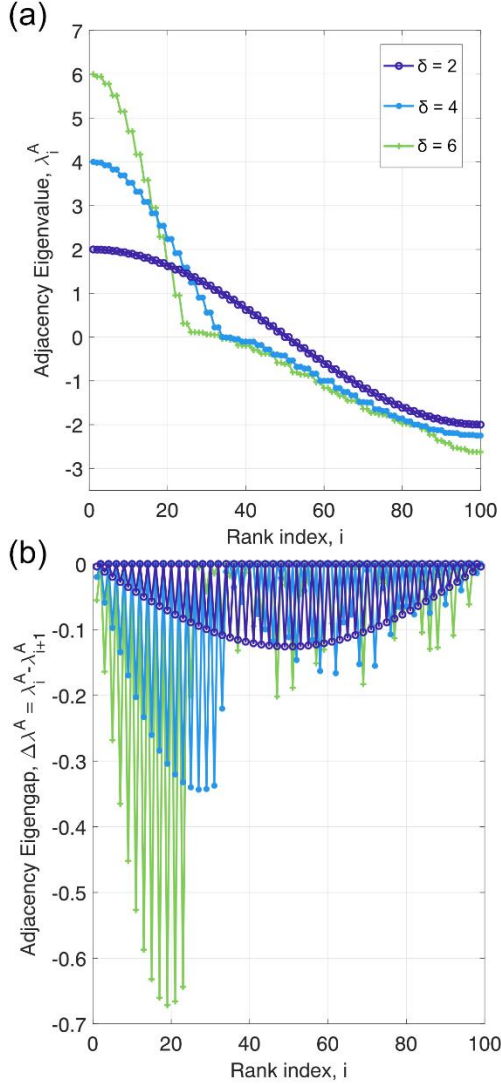


Fig. 1: (a) Adjacency and (b) adjacency eigengap spectra of 100-node ring with  $\delta_R = \{2, 4, 6\}$ .

Node connectivity across the rings is symmetrical, with nodes connecting to  $(\delta_R/2)$  nodes on either of their sides. Note that no clear community structure is observed (Fig. 1), with no single eigengap dominating the spectra.

This distinct eigenspectrum – fingerprint – makes ring networks a useful foundation upon which to study community formation as it can be dismissed from the studied networks' own eigenspectra. Note that increasing connectivity shifts the location of the largest eigengaps as well as increases their magnitude, which will influence analyses when structures are embedded upon the rings.

### C. Simulation Setup

To uncover the insights and interplay of the adjacency and Laplacian spectra, two sets of analyses are performed. The first set investigates artificially created networks comprised of a ring with groups of highly connected nodes on the ring, resulting in unevenly distributed nodes forming hubs on the ring; herein referred to as an aggregated ring. The second set of analyses are performed over networks consisting of intersecting rings, where hubs naturally emerge at the point of intersection. These networks are extracted from the modelling of satellite networks.

The aggregated ring networks are created by taking the adjacency matrix of a simple ring of varying indegree,  $\delta_R$ , and selecting a group of sequential nodes to interconnect, or aggregate. This results in the creation of a connected hub on the ring, representing a small complete graph on the ring. Analyses are performed for four scenarios,  $S_k$ , of increasing hub count,  $c$ . Simulations are performed on all networks with first one hub, then two, then three, and finally four hubs placed on the ring. Simulations are defined as,

$$S_k = \{(h_k)_{k=1}^{c=[1,4]}: |h_k| \in R\}, \quad (5)$$

where  $|h_k|$  is the size of the hubs, as specified by the analysis scenario parameters.

The intersecting rings consist of rings of fixed connectivity  $\delta_R$ , with a common focus, whose planes intersect and are not coincident. Analyses are shown for networks composed of 200-nodes spread across two rings and 210-nodes spread across three rings. Unlike the aggregated ring networks, these intersecting rings are extracted from satellite communication networks. Satellites equipped with Inter-Satellite Link (ISL) sub-system can communicate when in range of each other. Networks can therefore be created from the contacts between satellites. Satellite ring networks are modelled by locating satellites at equal angular intervals on a ring. Herein, for a fixed ISL range, the denser the ring, the higher the network's connectivity. Note that this is not typically the case for real satellite networks, where an upper limit on the number of open connections is fixed. Network connectivity is adjusted by changing the satellites' orbiting altitude, requiring the same number of satellites to be closer together as the altitude is lowered. When two satellite rings intersect, hubs are naturally created at this intersection as satellites from one ring enter into range of satellites from the other ring.

As a result of the network's dynamics, the hubs created at the rings' intersections are not necessarily symmetric: nodes on different side of the hubs may have different indegrees depending on satellite motion. To mitigate against this effect, where instantaneous connections may not reflect the actual network structure which would create noisy results, analyses are instead performed over time-averaged adjacency and Laplacian matrices,  $\bar{M}$ . These matrices are calculated as the mean of the time-dependent connections,  $M(t)$ , over time windows,  $tw$ , comprising of multiple time steps,  $\tau$ . Herein,  $\tau = 10$  is used as it has been found to offer a balance against the effect of

instantaneous connections, while limiting the extent of the averaging such that the networks' structure remains comprehensible.

$$\bar{M} = \frac{1}{tw} \cdot \sum_{\tau=1}^{tw} M(t + \tau) \quad (6)$$

### III. RESULTS & DISCUSSION

Aggregated ring networks are used to gain intuitive insights on structure and influence gained from adjacency and Laplacian matrices. The observations and intuitions built therefrom are then applied to the case study of intersecting ring networks.

Rings networks create very distinct eigenspectra (Fig. 1). The introduction of hubs affects and disturbs the observed patterns within their eigenspectra. Most notably, the embedding of hubs onto the ring networks result in the differentiation of the adjacency spectrum from the Laplacian's where before they were the same (Fig. 2, Fig. 3, and Fig. 4).

#### A. Structure

The adjacency eigenspectrum highlights dominant structures present on the network. To demonstrate this aggregated ring networks with one, two, three, or four hubs of ten interconnected nodes are compared in Fig. 2, which show the adjacency spectra of each. The rings have a connectivity of  $\delta_R = \{2, 4, 6\}$ , with all hubs comprising ten nodes ( $|h_k| = 10$ ). The network's modal connectivity remains equal to that of the rings.

The simulation is defined as

$$S_\alpha = \{(h_k)_{k=1}^{c=[1,4]} : |h_k| = 10\}, \quad (7)$$

where  $h_k$  is the set of nodes belonging to hub  $k$ , and  $|h_k|$  the size of the hubs. Analyses are



performed sequentially, first looking at adjacency spectrum when  $c = 1$ , meaning only one hub on the ring, up to  $c = 4$ , meaning that there are four hubs aggregated on the ring,  $k = \{1, 2, 3, 4\}$ .

For clarity, the results of the adjacency spectra shown in Fig. 2 are truncated to show only the first twenty of the 200 eigengaps as the remainder of the spectra provides little relevant information.

As seen across Fig. 2 (a) to (d), the largest adjacency eigengap,  $\Delta\lambda_{\max}^A$ , corresponds to the aggregated ring networks' hub count. These gaps appear as a discontinuity between the hubs' spectrum and the spectrum of a simple ring of equivalent indegree. The first eigenvalues are those of the hubs. As per the known lemma:  $\text{mean}(\delta) \leq \lambda_1^A \leq \max(\delta)$  (derived from the Rayleigh quotient [33, 34]), these first eigenvalues take on values between the networks' maximum in-degrees (found at the hub) and the network's average indegree. The largest eigenvalue thus increases with connectivity as both the upper and lower bound of the lemma increase.

As observed in Fig. 2 (a) to (d), the presence of the hubs disrupts the natural ring's eigenspectrum (Fig. 1). When hubs are introduced, the eigenvalues following the hub-induced discontinuities are shifted to the right as the hubs become the most dominant structure detected by the spectrum, resulting in the ring's natural spectrum being compressed. The eigenvalues group themselves in sets of  $c$  nodes, where  $c$  is the number of hubs in the networks. This grouping is observed in the eigengap spectra, with periodic oscillations to and fro zero. As such, for the three-hub case, the significant non-zero eigengaps,  $\Delta\lambda^A$ , occur every three indices at  $i = \{6, 9, 12, 15 \dots\}$  rather than every two indices as is typically observed in simple ring networks. Similarly, for four hubs, these gaps peak at indices  $i = \{4, 8, 12, 16 \dots\}$ . It can also

be noted that as the ring connectivity increases from  $\delta_R = 2$  to  $\delta_R = 6$ , the magnitude of the most significant eigengap  $\Delta\lambda_{\max}^A$  decreases, indicating the diminishing impact of the hub on the network as the hub's connectivity becoming less important relative to the ring's own connectivity.

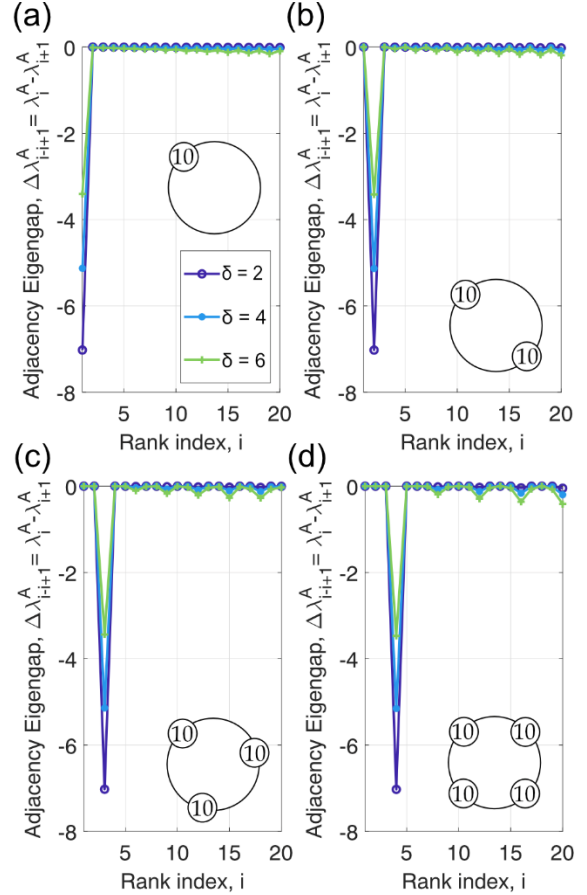


Fig. 2: **Adjacency** eigengap spectra of 200-node ring, connectivity  $\delta_R = \{2, 4, 6\}$ , with an increasing number of hubs,  $c = [1, 4]$ .

The adjacency eigenspectra highlight the size order of the structures present on the rings. This is shown by the eigengaps of Fig. 3. In this set of simulations, hubs in different combination of sizes are embedded on rings of connectivity  $\delta_R = 4$ . The changes to the corresponding adjacency spectra are explored when one, two, three, and four hubs are introduced to the ring,  $c = [1, 4]$ . The four analyses are each performed

for three simulated networks with different hub sizes. The simulations comprise of  $k$  hubs of size  $|h_k|$ , where  $k = [1, c]$ . The first simulation,  $S_1$ , consists of a ring embedded with up to four small hubs with similar numbers of nodes (Eq. (8)). The second,  $S_2$  (Eq.(9)), and third,  $S_3$  (Eq. (10)), simulations look at a case where one hub is either much smaller or much bigger than the others respectively.

The results of these simulations, shown in Fig. 3, are truncated from rank  $i = 1$  to  $i = 10$  to show only the section of the eigenspectra relating to the prominent network structures. Analyses are performed sequentially for each simulation, such that the impact of adding each new hub to the ring network can be tracked, starting from a single hub  $c = 1$  in Fig. 3 (a.i), (b.i), and (c.i), until four hubs are included in Fig. 3 (a.iv), (b.iv), and (c.iv).

$$S_1 = \left\{ (h_k)_{k=1}^{c=[1,4]} : |h_k| = \{10, 11, 12, 13\} \right\}, \quad (8)$$

$$S_2 = \left\{ (h_k)_{k=1}^{c=[1,4]} : |h_k| = \{10, 16, 17, 18\} \right\}, \quad (9)$$

$$S_3 = \left\{ (h_k)_{k=1}^{c=[1,4]} : |h_k| = \{20, 10, 11, 12\} \right\}, \quad (10)$$

If hubs are identical (Fig. 2), a single non-zero eigengap,  $\Delta\lambda_{\max}^A$ , develops at a rank corresponding to the hub count. If hubs have different sizes (Fig. 3), all eigengaps prior and up to the rank of the hub count are non-zero. As observed from the different simulations, the eigengaps' magnitudes and the rank at which the most significant gap is found depend on the relative sizes of the hubs.

When hubs have similar sizes, as is the case for  $S_1$  (Fig. 3 (a)), the most significant eigengap

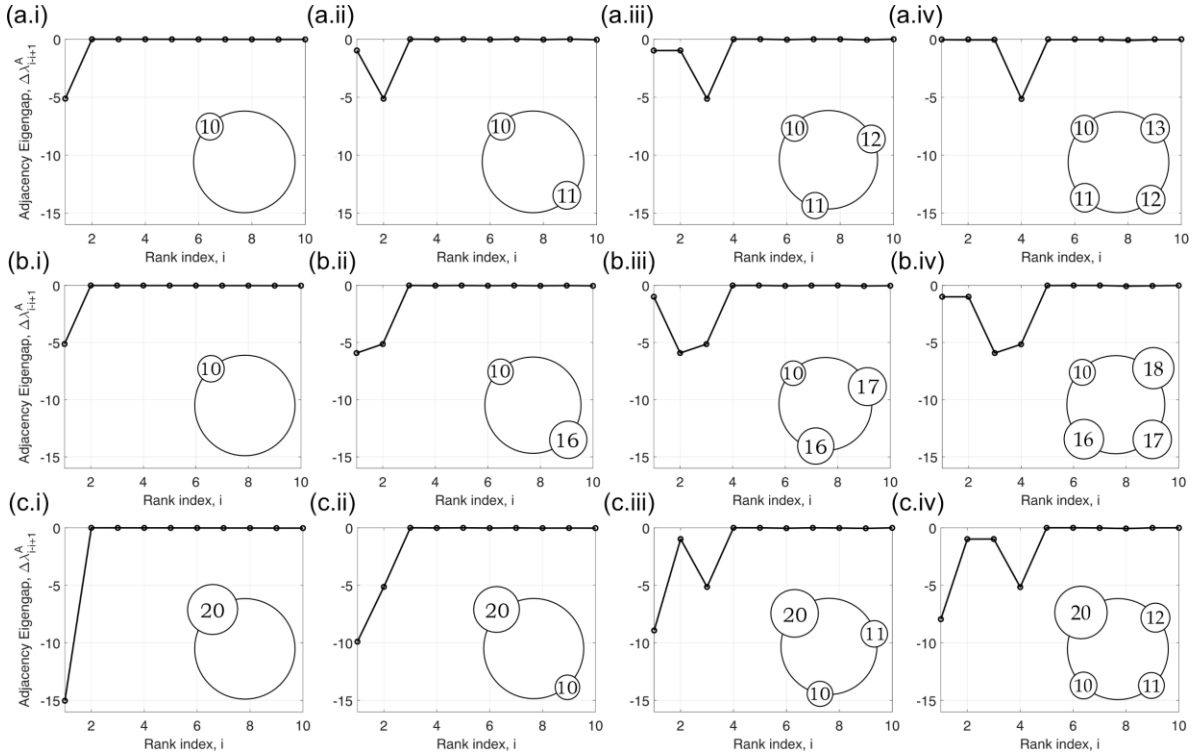


Fig. 3: **Adjacency** eigengap spectra of a 200-node ring, connectivity  $\delta_R = 4$ , with an increasing number of hubs,  $c = [1, 4]$ , of different sizes, (a)  $S_1$  (10, 11, 12, 13), (b)  $S_2$  (10, 16, 17, 18), and (c)  $S_3$  (20, 10, 11, 12).



corresponds to hub count,  $c$ . However, unlike the case where the hubs have the same size (Fig. 3), all eigengaps prior to  $\Delta\lambda_{\max}^A$  are also non-zero. Note that the final gap's magnitude depends on the size of the smallest hub such that for  $S_1$ , the final gap always has the magnitude of the 10-node hub.

When one hub is either much smaller or much larger than the others, the adjacency spectrum reflects this diversification in hub sizes: the most significant eigengap is no longer at the hub count. Instead, the largest eigengap is found at the rank corresponding to the largest or set of largest structures present on the network. For  $S_2$  (Fig. 3 (b)), one hub is significantly smaller than the others. Consequently, when  $c = 4$ , the other three hubs (16-, 17-, and 18-node hubs), form a set of larger structures detected in priority leading to the  $\Delta\lambda_{\max}^A$  occurring at a rank of  $i = 3$  (Fig. 3 (b.iv)). If only two of the large hubs are present (Fig. 3 (b.iii)), the  $\Delta\lambda_{\max}^A$  develops at rank  $i = 2$ . Here again, the final gap at  $i = c$  is dictated by the size of the smallest hub ( $|h| = 10$ ). The priority detection of large structures by the adjacency spectrum is similarly observed in  $S_3$  (Fig. 3 (c)). Therein, the much larger 20-node hub is always detected in priority with the most significant eigengap always appearing at rank  $i = 1$ . As new hubs are added, this first gap's magnitude decreases and a second significant gap at  $i = c$  develops corresponding to the detection of all hubs (Fig. 3 (c.ii)-(c.iv)).

The adjacency eigenspectra consistently highlight the most dominant structures of the network, identifying the number of hubs present on the rings with the magnitude of the gaps capturing the relative dominance of structures with respect to each other. The adjacency does not provide information on the number of nodes in each hub. If the hubs have the same size (Fig. 3), they are detected by a single non-zero significant adjacency eigengap. If multiple hubs of different sizes are embedded on the rings (Fig.

3), all adjacency eigengaps up to the number of hubs are non-zero. The largest eigengap indicates the largest hub or group of hubs, with the magnitude of the final eigengap indicating the size of the smallest hub.

## B. Influence

Where the adjacency eigenspectra highlight salient structures, the Laplacian spectra detect spanning tree roots in the order of their influence, wherein node connectivity begets influence. Herein, spanning trees are undirected subgraphs connecting a node to other hub nodes via a single path. Fig. 4 shows an aggregated ring network, with four sets of hubs of varying sizes, of 200-nodes and of connectivity  $\delta_R = 4$ . The simulations are  $S_\alpha$  (Eq. (7)),  $S_1$  (Eq. (8)),  $S_2$  (Eq. (9)), and  $S_3$  (Eq. (10)), all of which were previously analysed for their adjacency spectra (Fig. 2 and Fig. 3), as well as a simulation. All the simulations comprise four hubs,  $c = 4$ .  $S_\alpha$  looks at four small hubs of 10-nodes each.  $S_1$ , consists of four small hubs with similar numbers of nodes, while  $S_2$  and  $S_3$  look at cases where one hub is either much smaller or much bigger than the others respectively.

The Laplacian spectra of the four simulations between ranks  $i = 1$  and  $i = 60$  are shown in Fig. 4 along with their associated eigenvector heatmaps, truncated to match the Laplacian spectra. Hub sizes are shown to the left of each heatmap.

As seen in Fig. 4, the Laplacian spectra noticeably differ from the adjacency spectra. Where the adjacency spectrum detects the hubs as single entities, the Laplacian decomposes the hubs into their component nodes and assesses their individual influence on the network. This is seen most clearly from the Laplacian's largest eigengap and its other non-zero eigengaps. Instead of occurring at the hub count, the  $\Delta\lambda_{\max}^L$  appear at ranks corresponding to the number of spanning tree roots existing within the network's salient structures. This is seen most clearly in Fig. 4 (a), for which  $\text{idx}(\Delta\lambda_{\max}^L) = 36$ , where  $\text{idx}(\Delta\lambda_{\max}^L)$  is the rank at which the most significant Laplacian eigengap occurs. This eigengap also corresponds to the discontinuity between the hubs' influence and the remainder of the ring's distinct spectrum (Fig. 1). Commonly understood to emphasise the number of communities in which it is easiest to partition a network [17], herein this gap indicates that nine spanning tree roots are detected per hub, with the four hubs ( $c = 4$ ) having the same number of nodes ( $|h_k| = 10$ ). The roots represent a

tree's effective reach. This gap is independent from ring connectivity, remaining fixed no matter the ring connectivity  $\delta_R$ . The detection of nine spanning tree roots is validated by changing the hub count: the most significant eigengap occurs at an index multiplied by the number of hubs placed on the ring. As such, it develops at ranks  $i = \{9, 18, 27\}$  if one, two, or three hubs are considered, where Fig. 4 shows the results of the  $c = 4$  case. For hubs of the same size, this behaviour can be formalised with the relation,

$$\text{idx}(\Delta\lambda_{\max}^L) = \sum_{k=1}^c (|h_k| - 1), \quad (11)$$

where  $\text{idx}(\Delta\lambda_{\max}^L)$  is the rank at which the most significant Laplacian eigengap occurs,  $c$  is the hub count, and  $|h_k|$  is the number of nodes contained in each hub.

The Laplacian's decomposition of the structures detected by the adjacency highlights the methodology behind the hub creation process, i.e. the aggregating of adjacent nodes. A feature of this artificiality is that two types of nodes are

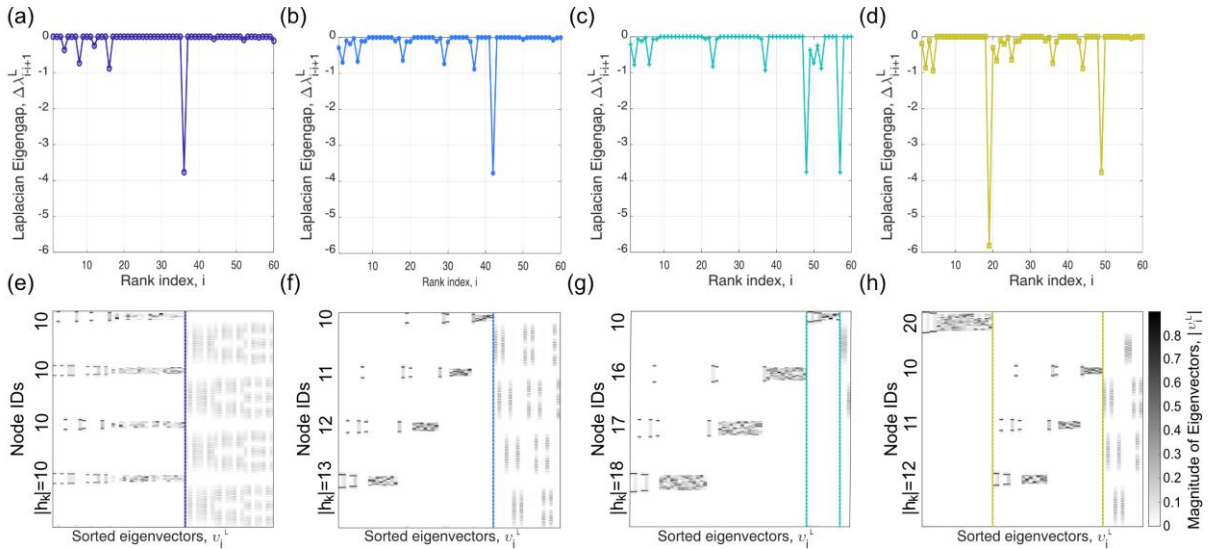


Fig. 4: **Laplacian** eigengap spectra and eigenvector's magnitude maps of a ring embedded with four hubs,  $c = 4$ . The embedded hubs have different sizes, (a)/(e)  $S_\alpha$  (10, 10, 10, 10), (b)/(f)  $S_1$  (10, 11, 12, 13), (c)/(g)  $S_2$  (10, 16, 17, 18), and (d)/(h)  $S_3$  (20, 10, 11, 12). The rings have 200 nodes and a connectivity  $\delta_R = 4$ . The largest and most significant eigengaps are shown by dashed lines on the eigenvector maps.

distinguished for each hub: “central” and “gateway” nodes. Central nodes are those nodes which only connect to other hub nodes, while gateway nodes connect beyond the hub. As such, central nodes have a degree equal to the number of other nodes in the hubs ( $|h_k| - 1$ ). In contrast, gateway nodes have a higher connectivity as they connect to central nodes and ring-nodes, acting as gateways to the hub and having influence over both the hub nodes and the ring-nodes. The gateway nodes’ exact degree depends on where they are on the hub border, with nodes most to the edge of the hub having the highest degree as they are connected to all other hub nodes as well as to  $\delta_R/2$  ring nodes for a total of  $\delta = |h_k| - 1 + \delta_R/2$ . The number of gateway nodes depends on the ring connectivity. Note that as the hubs are symmetrical, gateway nodes come in pairs with both nodes in the pair having the same degree.

As observed in Fig. 4 (a), central and gateway nodes are detected differently by the Laplacian’s eigenspectra. Gateway pairs appear as the smaller eigengaps occurring at the start of the spectrum, with the each non-zero eigengaps corresponding to a gateway pair. In this set of simulations, the ring’s connectivity of  $\delta_R = 4$ , results in four gateway nodes being created for each hub ( $\delta_R/2$  nodes on each side of the hub). As a result, four eigengaps are detected at the start of the spectrum, one at rank  $i = 4$ , another at  $i = 8$ , a small one at  $i = 12$ , and the largest at  $i = 16$  indicating all the combined gateway nodes. These observations are confirmed by Fig. 4 (e) which shows the absolute magnitude of the eigenvectors, sorted in the same order as the eigenspectrum from most dominant (left) to least (right). The heatmap confirms the hubs’ decomposition with node and node pairs highlighted in order of their connectivity such that outer most gateway nodes rank first. Note

that the eigenvectors entries of the gateway pairs’ nodes have equal amplitudes but opposite polarities (not shown in the plot). If plotted, it can be observed that if one of the gateway nodes takes on a positive amplitude, the hub’s second gateway node takes on the same value with a negative polarity, identifying the two nodes as a pair. Central nodes are detected thereafter as a single block. The transition between the central nodes and the ring’s harmonic patterns, that is the concentric circles, corresponds to the spectra’s most significant eigengap,  $\Delta\lambda_{\max}^L$ .

When the ring is embedded with hubs of different sizes, the Laplacian eigenspectrum becomes more complex. However, the same basic structure is observed. Each hub possesses a unique pattern of Laplacian eigengaps, a fingerprint, corresponding to its nodes’ influence. These fingerprints correspond to the spanning tree developing within the hubs and sorts them according to their relative reach. As a result, if the hubs have the same (Fig. 4 (a) and (d)) or approximately the same size (Fig. 4 (b) and (f)), their spectral fingerprints intermingle and the dominant eigengap corresponds to the total number of spanning tree roots found across all hubs. Thus for  $S_1$ ’s spectrum, a single dominant eigengap occurs at rank  $\text{idx}(\Delta\lambda_{\max}^L) = \sum_{k=1}^4 (|h_k| - 1) = 42$  following Eq. (11). The smaller eigengaps detected to the left of  $S_1$ ’s spectrum (Fig. 4 (b)) correspond to gateway nodes identified in order of their connectivity. As such, the first gap at  $i = 2$  corresponds to the two most highly connected nodes ( $\delta = 14$ ), while the gap at  $i = 6$  indicates the four nodes of connectivity  $\delta = 13$ .

If the hubs are sufficiently differentiated,  $S_2$ ’s and  $S_3$  (Fig. 4 (c) and (d)), their spectral fingerprints separate cleanly. As such, multiple significant eigengaps develop, corresponding to

the sets of hubs detected. In the fourth simulation, the much larger 20-node hub has a clear fingerprint with a spanning tree detected at  $i = 19$  (see Eq. (11)). The smaller hubs' ( $|h| = \{10, 11, 12\}$ ) spectra produce a combined eigengap at  $i = 19 + \sum_{k=1}^3 (|h|_k - 1) = 19 + 30 = 49$ , corresponding to the sum of the three hubs' individual spanning tree roots detected after the larger 20-node hub. This shift is validated by the eigenvector mapping (Fig. 4 (g)) which shows the smaller hubs' spectra interweaving with each other and appearing to the right of the 20-node hub. A similar spectral behaviour is observed in Fig. 4 (c) and (g) with the smallest 10-node hub separating cleanly from the intermingled spectra of larger hubs,  $|h| = \{16, 17, 18\}$ . The set of larger hubs are detected first with the network's most significant eigengap occurring at a rank  $\text{idx}(\Delta\lambda_{\max}^L) = \sum_{k=1}^3 (|h|_k - 1) = 48$ , as per Eq. (11), with the smaller hub being detected at rank  $i = 48 + 9 = 57$ .

### C. Structure and Influence

Intersecting ring networks provide appropriate case studies of the application of knowledge gained from the previous sections. These analyses confirm that although both the adjacency and the Laplacian provide relevant network insights when analysed independently, it is together that they provide the most complete picture of the network. Two networks are analysed: one comprising two rings and one of three rings, shown respectively in Fig. 5 (a) and (b). These Walker-Delta satellite rings are modelled with ISL ranges of 4000 km and inclinations of 56 degree, resulting in a ring connectivity of  $\delta_R = 4$ . The two ring satellite constellation consists of 200 (100 per ring) satellites at all altitude of 4 000 km while the

three-ring network consists of 210 satellites (70 per ring) at all altitude of 10 000 km.

Both constellations are modelled using the “sdp4” orbit propagator for a period of five hours with a step size of ten seconds. The networks are averaged over ten timesteps as per Eq. (6). Note that due to the time averaging, connectivity between nodes takes on non-integer values, making the graph edges weighted. For the two rings network, two hubs emerge from the rings' intersection for a hub count of  $c = 2$ . For the three rings network six hubs,  $c = 6$ , are created at the three rings' intersections. A key difference from the aggregated ring networks is that for intersecting ring networks, nodes with the highest connectivity are those closest to the rings' intersections and therefore the centre of the hubs.

The results of the adjacency and Laplacian analyses of both networks are shown in Fig. 5 (c) and (d), truncated to only show the features of interest. Like for the aggregated rings, the intersecting rings' adjacency and Laplacian spectra differ, with the adjacency giving insight in the prominent structures of the network and the Laplacian providing a decomposition of the network' influence patterns. As expected (Fig. 5 (c)), the largest adjacency eigengaps occur at ranks  $\text{idx}(\Delta\lambda_{\max}^A) = 2$  and  $\text{idx}(\Delta\lambda_{\max}^A) = 6$  for the two and three ring networks respectively, indicating that two and six hubs are identified as salient structures in each of the networks. Fig. 5 (c) also confirms what can be observed visually: the hubs have the same size as a single non-zero eigengap is detected. Once again, the spectra provide no further information regarding the size and internal structure of the hubs.

The Laplacian decomposes the hubs' internal structure created from the variation in their component nodes' connectivity, and provides insight into the nodes' pattern of influence, best contextualised by the findings of the adjacency spectrum. The internal structure is shown through the Laplacian eigengap spectra (Fig. 5 (d)) and the eigenvector's magnitude mapping (Fig. 5 (e) and (f)). The latter show the absolute

magnitude of the eigenvectors, sorted according to their associated eigenvalues' magnitudes, with vectors most to the left being associated with dominant eigenvalues. Of note, although the two rings' intersection results in two hubs, the eigenvector mapping (as plotted) shows four hubs (Fig. 5 (e)), while the three-rings mapping shows twelve hubs (Fig. 5 (f)). This is the result of node IDs being plotted in descending order, such

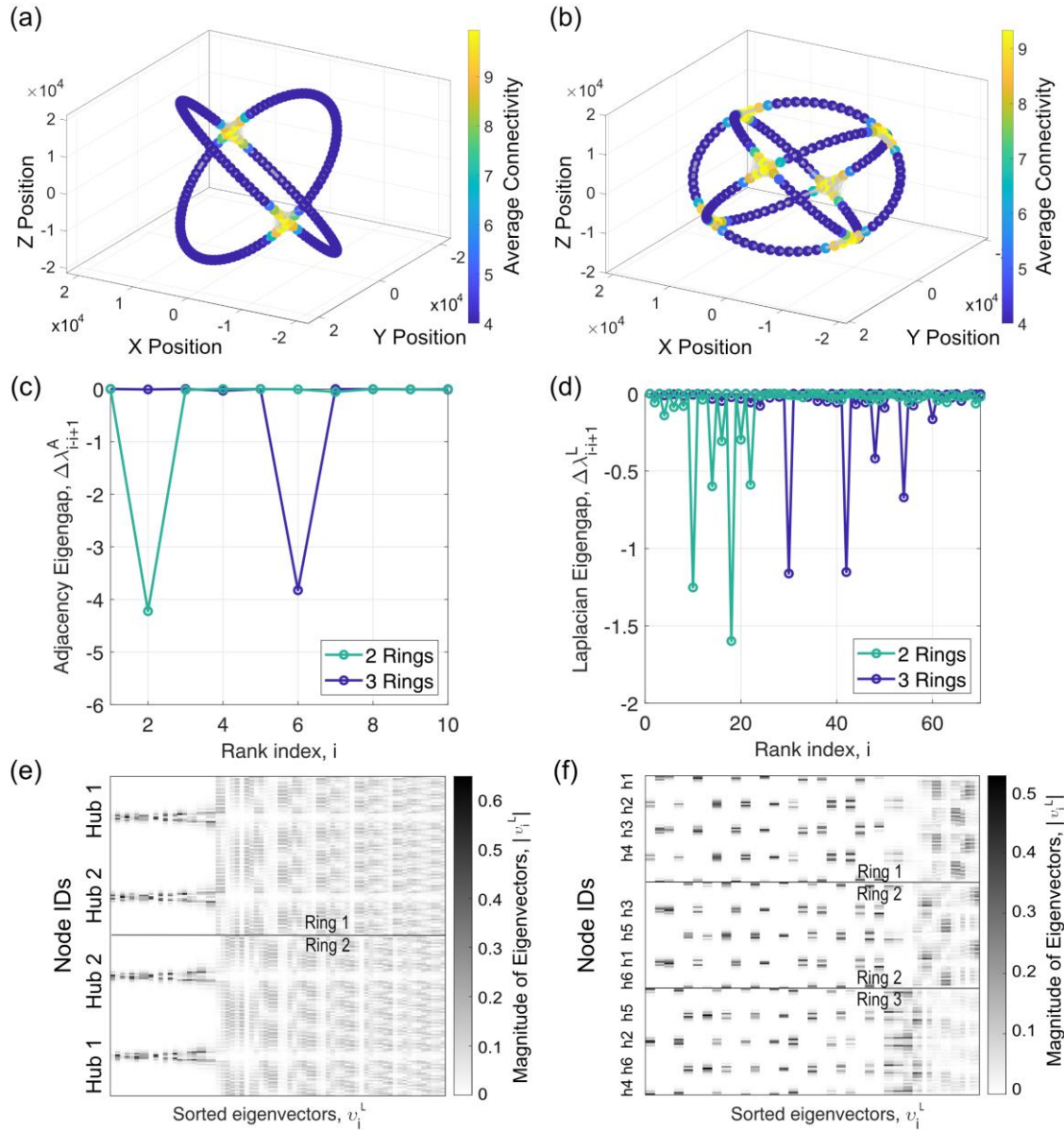


Fig. 5: Intersecting ring networks, their eigengap spectra, and their eigenvectors' magnitude. (a) two rings network with connectivity  $\delta = 4$ , (b) three rings network with connectivity  $\delta = 4$ , (c) adjacency eigenspectra, (d) Laplacian eigenspectra, and Laplacian eigenvectors' magnitude mapping of the (e) two- and (f) three-rings networks.

that for the two rings network, nodes 1 to 100 belong to the first ring and nodes 101 to 200 to the second ring, while for the three rings network node 1 to 70, 71 to 140, and 141 to 210 all belong to different rings. Hubs, which come at the intersection of two rings, are detected across both intersecting rings and as such, appear across both rings' eigenvector mapping. The hubs themselves can be identified by the pairing of nodes across the various eigenvectors: nodes belonging to one hub are highlighted by the same eigenvector, while nodes belonging to the second hub are highlighted at the next index. This behaviour is most apparent when looking at indices  $i = 1$  and  $2$  of Fig. 5 (f): rank  $i = 1$  highlights nodes belonging to one hub (meaning a node group including nodes from the first and second rings), while  $i = 2$  highlights the other hub. Note that the visual identification of heatmaps' hubs is dependent on the correct association and ordering of the nodes' IDs.

In contrast with the aggregated rings, the intersecting rings present a more organic structure (Fig. 5 (e) and (f)), with hubs seeing increased connectivity the closer their nodes are to the rings' intersections. This is reflected by the influence profiles detected by the networks' Laplacian spectra: the most influential communities are those found at the hubs' centres, while "gateway" nodes surrounding these influential "central" nodes are ranked thereafter, forming two nested communities. Central nodes encompass those nodes that are highlighted by eigenvectors spanning rank  $i = 1$  to that of the first of the two significant eigengaps (Fig. 5 (d)). The gateway nodes surrounding the central nodes are detected by the vectors between the first significant eigengap and the most dominant gap at  $\text{idx}(\Delta\lambda_{\max}^L) = 18$  and  $i = 42$  for the two and three ring networks respectively. Together, the

gateway and central nodes form the hubs' cores. Like for the aggregated rings, the most significant gaps correspond to the number of spanning tree roots, detected in the hubs as per Eq. (11). Thus, for the two rings network ( $c = 2$ ), ten nodes form each of the two hubs' core, resulting in a gap at  $\text{idx}(\Delta\lambda_{\max}^L) = \sum_{k=1}^c (|h|_k - 1) = 18$ . Correspondingly, for the three ring networks ( $c = 6$ ), the eight core nodes are detected by a spike at  $i = 42$ . Note that the hubs

The hubs' organic development is observed through the lack of visually definite transition between node communities (Fig. 5 (e) and (f)), unlike the aggregated hubs for whose community transitions were marked by significant eigengaps (Fig. 4).

In addition to core nodes, the hubs also encompass some few nodes with limited connectivity existing at the hubs' edges. These nodes are the reason as to why the intersecting rings' most significant eigengaps  $\Delta\lambda_{\max}^L$  do not mark the transition between the hubs and the undisturbed rings' spectra as is the case for the aggregated rings (Fig. 5 (e) to (h)). Instead, as seen in Fig. 5 (d), the eigengaps  $\Delta\lambda_{\max}^L$  are followed by non-zero eigengaps. These gaps account for the external nodes whose degrees are only slightly higher than the modal ring connectivity  $\delta_R$ . For the two rings network, the final gap occurs at  $i = 22 = \text{idx}(\Delta\lambda_{\max}^L) + 4$ , which includes two external nodes for each hub (Fig. 5 (e)). For the three ring networks, the gap at  $i = 42 = \text{idx}(\Delta\lambda_{\max}^L) + 24$  includes four external nodes for each of the six hubs (Fig. 5 (h)).

The hubs' internal structures are more clearly visible when plotting the networks coloured by the nodes' normalised eigenvectors' magnitudes as per Eq. (3). This plotting allows for the influence of the central and gateway nodes to be highlighted. Focusing on the two rings network,



the network's central and gateway nodes can be distinguished (Fig. 6 (a) and (b)), with the hubs' cores highlighted in Fig. 6 (c). It can be seen in Fig. 6 (a) that the central nodes are not actually at the rings' intersections, but rather, because of the averaging process, at a point between the rings in the direction of the nodes' movement. It can also be noted from Fig. 6 (a) and (b) that the transition from central to gateway node is not clear as there exists some overlap between the two sets of nodes. This pattern is indicative of the fact that the hubs developing at the rings' intersections form organic, dynamic, and nested communities unlike the artificial hubs of the aggregated rings. When part of the intersecting rings' networks, nodes are on a spectrum of connectivity and influence and as such, can belong to both communities of central and gateway nodes. If no time averaging is performed over the network ( $tw = 1$  as per Eq. (6)), this effect becomes more apparent: the spectrum is noisier as multiple potential community partitions/groupings are detected instead of simply identifying central and gateway nodes. Note that the number of core nodes remains the same with the dominant eigengaps remaining at  $\text{idx}(\Delta\lambda_{\max}^L) = 18$  and  $i = 42$  for the two and three ring networks. Increasing the averaging time window duration (as is the case in Fig. 5) only coalesces the smaller communities

together as the heterogeneous indegree distribution is smoothed into two clear groups: central and gateway nodes. Still, the distinction between the nodes remains a porous one and nodes can appear to belong to both communities.

The adjacency and Laplacian spectra of complex networks are best interpreted together: a network's adjacency spectrum provides key information regarding the salient structures present on the network and their relative sizes but nothing regarding the number of nodes present in those structures, nor their relative connectivity. In contrast, the Laplacian spectrum decomposes these structures and provides insight regarding which nodes have the most influence and how this influence is spread across the hubs. When considering the time-averaged two and three ring networks, two nested communities are detected with two significant eigengaps, with the gaps occurring at the higher ranks corresponding to the number of spanning tree roots in each of the intersecting rings' hubs' cores. The detected community nesting highlights the complexity in synchronising intersecting rings. These networks not only need to cope with the looped signal transmission of ring networks which often result in chaotic synchronisations [23], but also with the interplay of topological scales present within the hub structures, where synchronisation

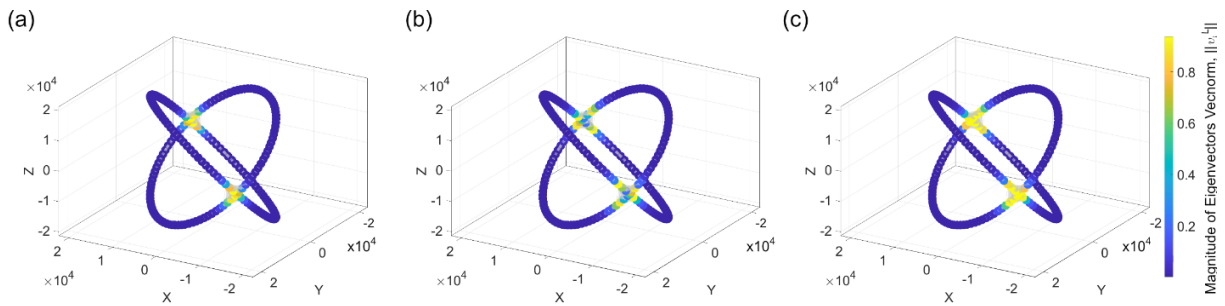


Fig. 6: Vector-wise norm of the Laplacian eigenvectors of the  $\delta = 4$  two rings networks for truncated matrix between (a)  $i = 1$  and  $i = 10$  (rank of second most significant eigengap), (b)  $i = 10$  and  $i = 18$  (rank of most significant eigengap), and (a)  $i = 1$  and  $i = 18$ .

typically follows topological scales [12]. Initial conditions are thus of crucial importance to the synchronisation process, as they dictate how the topological clusters develop, congregate, and possibly come to a consensus with each other.

## IV. CONCLUSION

Comparative analyses of adjacency and Laplacian eigengap spectra of ring-based networks confirms the established knowledge that where the adjacency matrix's spectrum reveals salient structures such as highly connected hubs, the Laplacian identifies nodes' influence. Thenceforth, the adjacency eigenspectrum is found to uncover the hierarchical ordering of structures on the basis of their relative sizes and the Laplacian identifies influence dependent on the effective reach of the spanning trees within salient structures. Laplacian eigenvector mapping further highlights the structures' community nesting which directs the synchronisation process. Although independent analyses of the adjacency and the Laplacian both provide insights into network characteristics, it is together that they uncover the structure and influence of networks' local and global features. The Laplacian spectrum details the internal structure of densely connected node clusters. However, these insights are underpinned by knowledge of the number and relative sizes of a network's salient structures: information provided and characterised by the adjacency spectrum.

## DECLARATIONS

### Data Availability

No data were created or analysed in this study.

## Acknowledgements

This work is funded by the Air Force Office of Scientific Research (AFOSR), Grant number FA8655-22-1-7033.

## Author Contributions

Conceptualisation and methodology, A.B., R.A.C., and M.M.; numerical investigation A.B.; interpretation, A.B., R.A.C., and M.M.; writing, review, and editing, A.B., R.A.C., and M.M.; funding acquisition, M.M and R.A.C. All authors have read and agreed to the published version of the manuscript.

## REFERENCES

- [1] S. Boccaletti, V. Latora, Y. Moreno, M. Chavez, and D.-U. Hwang, "Complex networks: Structure and dynamics," *Physics reports*, vol. 424, no. 4-5, pp. 175-308, 2006.
- [2] J. A. Acebrón, L. L. Bonilla, C. J. Pérez Vicente, F. Ritort, and R. Spigler, "The Kuramoto model: A simple paradigm for synchronization phenomena," *Reviews of modern physics*, vol. 77, no. 1, pp. 137-185, 2005.
- [3] S. Boccaletti, J. Kurths, G. Osipov, D. Valladares, and C. Zhou, "The synchronization of chaotic systems," *Physics reports*, vol. 366, no. 1-2, pp. 1-101, 2002.
- [4] L. M. Pecora and T. L. Carroll, "Synchronization of chaotic systems," *Chaos: An Interdisciplinary Journal of Nonlinear Science*, vol. 25, no. 9, 2015.
- [5] J. Gómez-Gardenes, Y. Moreno, and A. Arenas, "Paths to synchronization on complex networks," *Physical review letters*, vol. 98, no. 3, p. 034101, 2007.
- [6] A. Arenas, A. Díaz-Guilera, J. Kurths, Y. Moreno, and C. Zhou, "Synchronization in

complex networks," *Physics reports*, vol. 469, no. 3, pp. 93-153, 2008.

[7] E. Schöll, "Synchronization patterns and chimera states in complex networks: Interplay of topology and dynamics," *The European Physical Journal Special Topics*, vol. 225, pp. 891-919, 2016.

[8] S. Ulonska, I. Omelchenko, A. Zakharova, and E. Schöll, "Chimera states in networks of Van der Pol oscillators with hierarchical connectivities," *Chaos: An Interdisciplinary Journal of Nonlinear Science*, vol. 26, no. 9, 2016.

[9] M.-Y. Zhou, Z. Zhuo, S.-m. Cai, and Z. Fu, "Community structure revealed by phase locking," *Chaos: An Interdisciplinary Journal of Nonlinear Science*, vol. 24, no. 3, 2014.

[10] M. E. Newman, "Finding community structure in networks using the eigenvectors of matrices," *Physical Review E—Statistical, Nonlinear, and Soft Matter Physics*, vol. 74, no. 3, p. 036104, 2006.

[11] C. Nathe, K. Huang, M. Lodi, M. Storace, and F. Sorrentino, "Delays induced cluster synchronization in chaotic networks," *Chaos: An Interdisciplinary Journal of Nonlinear Science*, vol. 30, no. 12, 2020.

[12] A. Arenas, A. Díaz-Guilera, and C. J. Pérez-Vicente, "Synchronization reveals topological scales in complex networks," *Physical review letters*, vol. 96, no. 11, p. 114102, 2006.

[13] C. Grabow, S. Grosskinsky, J. Kurths, and M. Timme, "Collective relaxation dynamics of small-world networks," *Physical Review E*, vol. 91, no. 5, p. 052815, 2015.

[14] F. M. Atay, T. Bıyıkoglu, and J. Jost, "Network synchronization: Spectral versus statistical properties," *Physica D: Nonlinear Phenomena*, vol. 224, no. 1-2, pp. 35-41, 2006.

[15] F. M. Atay, T. Bıyıkoglu, and J. Jost, "Synchronization of networks with prescribed degree distributions," *IEEE Transactions on Circuits and Systems I: Regular Papers*, vol. 53, no. 1, pp. 92-98, 2006.

[16] A. Raza and M. M. Munir, "Insights into network properties: spectrum-based analysis with Laplacian and signless Laplacian spectra," *The European Physical Journal Plus*, vol. 138, no. 9, p. 802, 2023.

[17] H.-W. Shen and X.-Q. Cheng, "Spectral methods for the detection of network community structure: a comparative analysis," *Journal of Statistical Mechanics: Theory and Experiment*, vol. 2010, no. 10, p. P10020, 2010.

[18] E. A. Monakhova, "A survey on undirected circulant graphs," *Discrete Mathematics, Algorithms and Applications*, vol. 4, no. 01, p. 1250002, 2012.

[19] X. Zhao, J. Liu, G. Chen, L. Chai, and D. Wang, "Dynamics and synchronization of complex-valued ring networks," *International Journal of Bifurcation and Chaos*, vol. 32, no. 05, p. 2230011, 2022.

[20] M. J. Panaggio and D. M. Abrams, "Chimera states: coexistence of coherence and incoherence in networks of coupled oscillators," *Nonlinearity*, vol. 28, no. 3, p. R67, 2015.

[21] S. He, K. Sun, and H. Wang, "Synchronisation of fractional-order time delayed chaotic systems with ring connection," *The European Physical Journal Special Topics*, vol. 225, no. 1, pp. 97-106, 2016.

- [22] E. A. Martens, E. Barreto, S. H. Strogatz, E. Ott, P. So, and T. M. Antonsen, "Exact results for the Kuramoto model with a bimodal frequency distribution," *Physical Review E—Statistical, Nonlinear, and Soft Matter Physics*, vol. 79, no. 2, p. 026204, 2009.
- [23] D. A. Wiley, S. H. Strogatz, and M. Girvan, "The size of the sync basin," *Chaos: An Interdisciplinary Journal of Nonlinear Science*, vol. 16, no. 1, 2006.
- [24] J.-C. Bermond, F. Comellas, and D. F. Hsu, "Distributed loop computer-networks: a survey," *Journal of parallel and distributed computing*, vol. 24, no. 1, pp. 2-10, 1995.
- [25] N. M. Choo, B. J. Lunday, D. K. Ahner, N. B. Gaw, B. D. Little, and B. K. McBee, "Investigating Regional Communication Network Robustness of an Asymmetric String-of-Pearls Satellite Constellation Design Framework," *Journal of Spacecraft and Rockets*, pp. 1-10, 2024.
- [26] J. G. Walker, "Continuous whole-earth coverage by circular-orbit satellite patterns," *Nasa Sti/recon Technical Report N*, vol. 78, p. 11169, 1977.
- [27] A. Bouis, R. A. Clark, and M. Macdonald, "An autonomous distributed timing signal in-space as alternative to GNSS time synchronisation," in *75th International Astronautical Congress*, 2024.
- [28] L. M. Marrero *et al.*, "Architectures and synchronization techniques for distributed satellite systems: A survey," *IEEE access*, vol. 10, pp. 45375-45409, 2022.
- [29] S. Fortunato, "Community detection in graphs," *Physics reports*, vol. 486, no. 3-5, pp. 75-174, 2010.
- [30] L. J. Grady and J. R. Polimeni, *Discrete calculus: Applied analysis on graphs for computational science*. Springer, 2010.
- [31] A. Ortega, *Introduction to graph signal processing*. Cambridge University Press, 2022.
- [32] R. M. Gray, "Toeplitz and circulant matrices: A review," *Foundations and Trends® in Communications and Information Theory*, vol. 2, no. 3, pp. 155-239, 2006.
- [33] C. Hoppen, D. P. Jacobs, and V. Trevisan, *Locating Eigenvalues in Graphs*. Springer, 2012.
- [34] D. Cvetković, P. Rowlinson, and S. Simić, *An introduction to the theory of graph spectra*. Cambridge University Press, 2009.